Generic inertia emulation controller for multi-terminal voltage-source-converter high voltage direct current systems

Zhu, Jiebei; Guerrero, Josep M.; Hung, William; Booth, Campbell D.; Adam, Grain P.

Published in:
IET Renewable Power Generation

DOI (link to publication from Publisher):
10.1049/iet-rpg.2014.0109

Publication date:
2014

Document Version
Early version, also known as pre-print

A generic inertia emulation controller for multi-terminal VSC-HVDC systems

Jiebei Zhu, Josep M. Guerrero†, William Hung-, Campbell D. Booth^, Grain P. Adam^*

** National Grid, UK. Email:Jiebei.zhu@nationalgrid.com*

†Aalborg University, Denmark. Email: Joz@et.aau.dk

-Independent Power System Consultant, UK. Email: ukwilliamhung@gmail.com

^University of Strathclyde, UK..Email: Campbell.d.booth@strath.ac.uk; Grain.adam@strath.ac.uk

Keywords: Virtual inertia, inertia emulation, frequency response, multi-terminal HVDC, MTDC, HVDC converters, HVDC transmission control, island mode.

Abstract

A generic Inertia Emulation Controller (INEC) scheme for Multi-Terminal Voltage-Source-Converter based HVDC (VSC-MTDC) systems is proposed and presented in this paper. The proposed INEC can be incorporated in any Grid-side Voltage-Source-Converter (GVSC) station, allowing the MTDC terminal to contribute an inertial response to connected AC systems during system disturbances, in a fashion similar to synchronous generators. The DC link capacitors within the MTDC are utilised by the INEC scheme to exchange stored energy with the AC system by varying the overall DC voltage level of the MTDC network within a safe and pre-defined range. A theoretical treatment of the INEC algorithm and its implementation and integration within a conventional VSC control system are presented, and the impact on the total DC capacitance required within the MTDC network to ensure that DC voltages vary within an acceptable range are discussed. The proposed INEC scheme is validated using a Matlab/Simulink model under various changes in demand and in response to AC network faults. The model incorporates a multi-machine AC power system connected to a MTDC transmission system with multiple converter-interfaced nodes. The effectiveness of the INEC in damping post-fault oscillations and in enhancing AC system frequency stability is also investigated. The system is shown to perform well and is attractive for providing a stable MTDC system that is capable of providing valuable support to the connected AC systems.

1 Introduction

The fast pace of the development of renewable power generation has raised many technical issues. A major concern associated with renewables energy resources is with respect to their limited capability to support system frequency management, when compared to conventional synchronous, directly-connected, power generation units. Power system frequency is a global indicator of the balance between active power generation and demand. Any short-term active power imbalance results in a change of system frequency; the rate of which varies depending on the nature of the disturbance, the prevailing system inertia and installed generation system capacity. In general, a higher value of aggregated system inertia leads to higher frequency stability and system security.

An increasing penetration of wind power generation may act to deteriorate system frequency stability. This is primarily due to two reasons:

i) Typical wind turbine generators (WTGs) have lower inertia than traditional synchronous power generation plant [1] and their inherent inertial response to changes in frequency is relatively reduced or even eliminated;

ii) The majority of wind turbine generators and other forms of renewable energy sources (e.g. fuel cells, tidal and wave power) use power electronic interfaces or HVDC links, decoupling the kinetic energy available from their prime movers, if any is indeed available [2].

Inevitably, reduced inertia presents a greater risk of instability requiring mitigation such as changes to control systems, requirements for greater amounts of spinning reserve and fast acting schemes such as pumped-storage hydro schemes, increased amounts of demand response or load shedding facilities, and more frequent starting of generation installed to support the system, which is often inefficient and costly to the system operator (and ultimately to consumers). To mitigate such negative impacts, many researchers have investigated the possibility of using WTGs to provide inertial and primary frequency response capabilities to the supplied systems [1]-[4], and the possibility of coordinating the HVDC transmission systems with the associated offshore wind farms to contribute inertia responses to the system by means of dedicated and separate communications facilities [5], or without dedicated communications media, using the physical DC cables as information channels [6]. However, these methods are proposed to either operate the wind power resource in “reserved” or “de-loaded” modes, which

obviously reduces the generation efficiency and/or reduces wind turbine rotor speeds at times of frequency disturbances, which can lead to difficulties in restoring normal rotor speeds [4] rapidly following system recovery. This could mean that, while a valuable short-term inertial response (e.g. in terms of a rapid temporary increase in active power output) may be achieved, this could be immediately followed by a reduced and sustained power output due to the extraction of energy from the rotors to support the inertial response, which may further compromise the system performance if a major problem is being encountered, such as the loss of a major infeed elsewhere in the system: such schemes may therefore effectively solve one problem but exacerbate another.

VSC-MTDC transmission systems, as an expansion of point-to-point VSC-HVDC systems, have been the focus of discussions and development in recent years. A VSC-MTDC offers attractive features such as flexibility of power dispatch and a reduction of the intermittency of renewable power as the system can be aggregated over extremely large geographical areas, resulting in larger and more predictable availability. When compared to point-point VSC-HVDC systems, MTDC facilitates the economical proliferation of renewable power through reducing the numbers of HVDC converter stations required and facilitating routes for offshore wind farms to integrate with onshore grids [7]-[9].

However, there are potential disadvantages: increasing deployments of VSC-HVDC/VSC-MTDC systems can act to segment inertia-rich AC grids into relatively smaller subsystems. This will obviously reduce regional system inertia/strength. A novel INEC strategy for VSC-HVDC transmission system was initially proposed using the energy storage capability of DC capacitors in [11]. As a follow-up to this, this paper extends the INEC application from a point-to-point HVDC system to MTDC configuration. The dynamic behaviour of the system under a variety of system scenarios has been studied using a multi-machine power system as shown in Fig.1.

2 Modelling and control a MTDC system

2.1 Characteristics of a VSC converter

VSC converters have very distinct electrical characteristics compared to synchronous machines [13]. These differences are summarised as follows:

i) Synchronous machines produce relatively low levels of total harmonic distortion (THD), as production of a sinusoidal voltage waveform is an inherent feature of the machine design, whereas VSC converters produce a sinusoidal voltage waveform by applying appropriate reference waveform to the modulators. The fast switching VSC system eliminates low-order voltage harmonics, but the resulting high-order harmonic components inherent in the output must be attenuated by filtering.

ii) Conventional synchronous machines adjust the voltage at the grid interface point using a closed-loop excitation control scheme within automatic voltage regulators, whereas VSC converters can control grid voltage magnitude at the point of common coupling autonomously. Voltage controllers of VSC converters have a relatively higher bandwidth compared with those used for synchronous machines.

iii) Fault current from synchronous machines is high due to low source impedance, and can be sustained for a relatively long period due to the robust mechanical and thermal designs inherent to synchronous machines. In contrast, the fault current from VSC converters is relatively low because of the limiting effect of the current controllers, and high fault currents must be avoided/limited as the semiconductor switches are vulnerable to high thermal stresses arising from exclusively high currents [13].

iv) The response of synchronous machines to step changes of system frequency are determined by the interactions between the directly-connected electrical and mechanical systems within the machine. A rapid drop of system frequency results in the initial delivery of energy stored in the rotating masses of the machine followed by control actions of turbine speed governors to increase (or reduce) the energy delivered to the prime mover. Similarly, an increase in system frequency would be initially resisted by the inertia of the machine, and the speed controller would subsequently act to reduce energy to the prime mover. Accordingly, synchronous machines inherently change their real power outputs to counteract changes in the frequency of the system. However, VSC converters are generally designed to track and follow the grid frequency, while maintaining the real power output to some pre-determined target level. VSC converters typically have no or little contribution to grid inertia, rotor angle and frequency stability [2]-[4], [11].

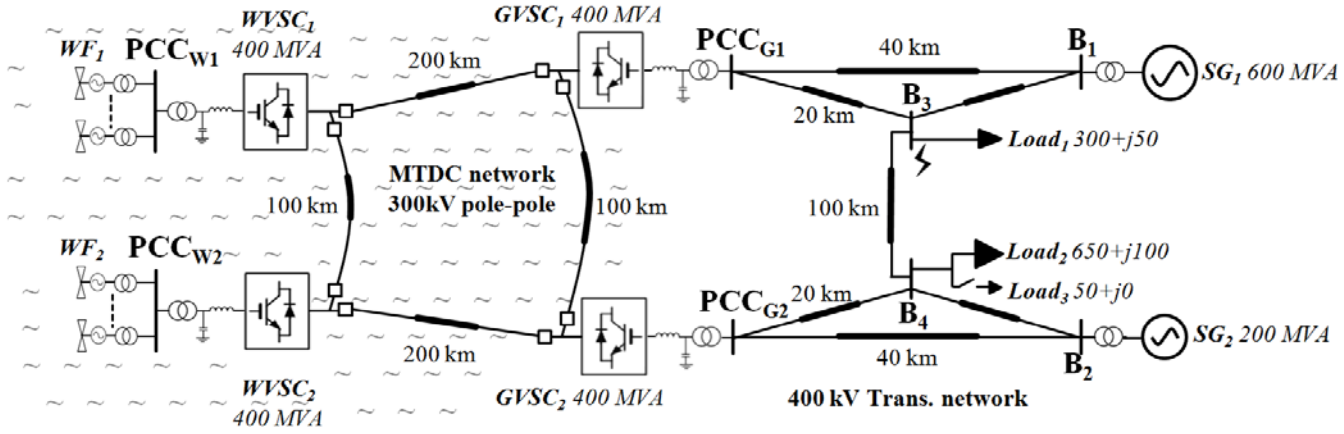

Fig. 1 *Test scenario for the INEC implementation in the MTDC system*

2.2 Configuration of the VSC-MTDC system under study

Fig. 1 shows a candidate MTDC configuration with four terminals. There are two independent wind power park modules (PPM) WF_1 and WF_2 injecting power into the MTDC network via converters $WVSC_1$ and $WVSC_2$ (400 MVA each). The WTG step-up transformers raise the 690 Volts nominal generator terminal voltage to 11kV, the offshore AC wind farm network voltage. This voltage is further raised to 150kV by the WVSC transformers before conversion to the DC network voltage of ±150kV by the WVSC converters. While the DC system is of a ring configuration, other DC network connections such as radial type would be possible. The converters at $GVSC_1$ and $GVSC_2$ deliver power to the 400kV AC transmission system on the right hand side of Fig 1 via the GVSC transformers. In the AC power system two synchronous machines (SG_1 600MVA, SG_2 200MVA) interconnect with three static loads ($Load_1$ 300WM+50MVar, $Load_2$ 650WM+100MVar, $Load_3$ 50MW). To demonstrate the effectiveness of the proposed MTDC INEC controller and investigate future power systems with significant amount of offshore wind power delivered by VSC-HVDC connections, the whole power system is designed in a way that the delivered offshore wind power via the MTDC network is comparable to that generated by the AC synchronous machines. The parameters for the entire system can be found in the Appendix.

The control modes for the GVSC and WVSC systems are normally different. The GVSC is controlled to export the power from the MTDC network into an established AC grid voltage, whereas WVSC aims to establish the offshore network voltage. The two control modes for GVSC and WVSC will be introduced in the following sections.

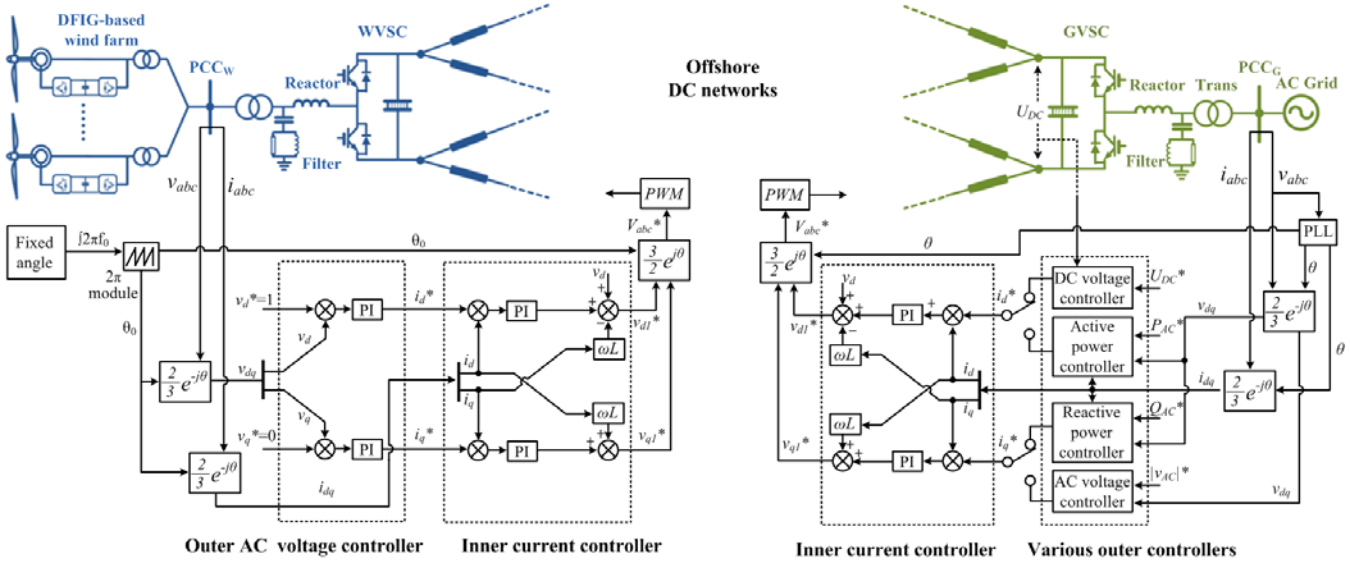

Fig. 2 *Control systems for WVSCs and GVSCs*

2.3 Control of GVSC

A grid-connected mode is employed for GVSC to export power from the MTDC network into the AC grid which has an established voltage. The objective of the GVSC control is to dispatch the wind power to the connected AC grids while simultaneously ensuring satisfactory DC voltage stability in the MTDC network. The control system for GVSCs consists of outer controllers (to control DC and AC voltage and for real and reactive power injected to the AC side) and an inner current controller, as shown on the left hand side of Fig. 2.

The AC-side dynamics of the converter can be expressed by the following equation:

$$v_{abc1} - v_{abc} = L\frac{di_{abc}}{dt} + Ri_{abc} \tag{1}$$

where v_{abc1} and v_{abc} represents the converter side and grid side voltages respectively, i_{abc} represents the three-phase currents flowing through the reactor and grid interface transformer, and L and R are the equivalent combined inductance and resistance of the phase reactor and transformer. A synchronous d-q reference approach is conventionally employed to facilitate VSC-HVDC control [8][12] The three-phase voltages v_{abc} and currents i_{abc} measured at the point of common coupling (PCC) are transformed to d-q components v_{dq} and i_{dq} via the Park Transformation [15][16]:

$$v_{dq} = v_d + jv_q = \tfrac{2}{3} je^{-j\omega t}(v_a + e^{j\frac{2}{3}\pi} v_b + e^{-j\frac{2}{3}\pi} v_c) \tag{2}$$

$$i_{dq} = i_d + ji_q = \tfrac{2}{3} je^{-j\omega t}(i_a + e^{j\frac{2}{3}\pi} i_b + e^{-j\frac{2}{3}\pi} i_c) \tag{3}$$

A phase-locked-loop (PLL) block [11] is used to synchronise the HVDC converter to the grid voltage at the PCC and to align the voltage vector of the grid with the d-axis (when the network voltage at the PCC remains constant and balanced, v_q=0). In the synchronous d-q reference frame, the dynamics of the VSC in (1) can be expressed as:

$$v_{d1} = L\frac{di_d}{dt} + Ri_d - \omega Li_q + v_d \tag{4}$$

$$v_{q1} = L\frac{di_q}{dt} + Ri_q + \omega Li_d \tag{5}$$

where v_{d1} and v_{q1} are the d-axis and q-axis converter side voltage vectors.

In order to track the reference currents i_d^* and i_q^*, the inner current control uses proportional-integral (PI) controllers with feedback to regulate the current vectors i_d and i_q as shown in Fig. 2. Therefore, the VSC voltage vector references v_{d1}^* and v_{q1}^* for the VSC are computed as follows:

$$v_{d1}^* = (k_p + \frac{k_i}{s})(i_d^* - i_d) + Ri_d - \omega Li_q + v_d \tag{6}$$

$$v_{q1}^* = (k_p + \frac{k_i}{s})(i_q^* - i_q) + Ri_q + \omega Li_d + v_q \tag{7}$$

where k_p and k_i are the PI controllers' gains.

The initial gains for the PI controllers can be selected by analysing the VSC's electrical characteristics, considering the impedance of the phase reactor and the grid interface transformer using Laplace manipulation [18]. However, the final gains must be properly tuned to ensure that satisfactory performance is achieved over the entire system operating conditions, which must be considered to include both AC and DC network faults [19]. The voltage vector references v_{d1}^* and v_{q1}^* are transformed to a three-phase value v_{abc1}^* for pulse width modulation (PWM) to produce the desired converter three-phase voltage. A double tuned AC shunt filter, tuned at the 27th and 54th harmonics in this case (1st and 2nd order of 1.35kHz VSC switching frequency), is installed between the phase interfacing reactor and transformer, with the phase interfacing reactor and converter transformer forming part of the

filtering network that filters high frequency harmonics.

The outer controllers, as illustrated on the right hand side of Fig. 2, are used to compute the reference current i_d^* based on an active power or DC voltage reference, and i_q^* is computed based on reactive power or grid AC voltage amplitude.

2.4 Control of WVSC

An island control mode is adapted for the WVSC to establish the offshore network voltage (in contrast to the GSVCs where the voltage of the system being supplied is already established). When the MTDC network is used to connect wind farms, the WVSCs act to set up a "stiff" AC bus with constant voltage and frequency to allow all individual WTGs to synchronise to the wind farm AC system, and transmit their generated power into the wind farm's AC grid, as shown in Fig. 2. The control of the wind farm is based on maximum power point tracking (MPPT), which is based upon wind power-versus-turbine speed characteristics at different wind speeds [8]-[12].

Various island modes for VSC control system are discussed in [13], and theoretically they are all suitable for MTDC WVSC control. The most distinct feature of a WVSC's control loops, from the perspective of operating in grid-connected mode when connected to a wind-farm's AC system, is that the angle used for abc-dq and dq-abc transformations is obtained from a signal oscillator with a fixed modulation rate, as shown in the saw-tooth block on the left hand side of Fig. 2, rather than from a phase-locked loop dynamically tracking the established grid frequency. This oscillator sets the frequency of the WVSC's voltage waveforms so the offshore electrical frequency is regulated (e.g. at 50/60 Hz). As illustrated in Fig.2, the d-axis voltage vector v_d, representing offshore voltage magnitude, is controlled at 1 pu, whereas q-axis voltage vector v_q, representing any offshore voltage phase angle change, is regulated at 0 so that offshore network frequency remains constant. As long as the frequency and AC voltage magnitude are maintained at constant levels, the power generated by the wind farm is automatically absorbed via the WVSC and transferred to the DC link [12].

In [8]-[12] and [14], a single-loop control approach to control of voltage in an islanded mode, in the absence of any inner current controller, is adopted for the integration of a doubly-fed-induction-generator-based (DFIG) wind farm to the offshore AC network. However, a shortcoming of this control approach, as discussed in [13], is that it

has no explicit current control capabilities to limit large transient currents, due to the absence of inner current control loops, and this could lead to unnecessary stress on the converters.

Inner current control loops, similar to that of the GVSC controllers, is therefore adoped in the WVSC as shown in Fig. 2 to provide a secure means of current control for the WVSC operation (also referred as "nested voltage and current control-loops" in [13]). By regulating the AC voltage amplitude component v_d with a target value of 1 pu and the phase angle voltage component v_q with a target of 0, the WVSC can act as a "stiff" voltage source and i_{dq}* for the inner current control is generated. A constant phase angle θ_0 is provided for the Park and inverse Park transformations by a fixed PLL which uses grid frequency f_0 (e.g. 50 Hz) as a constant input, as illustrated in Fig. 2.

3 Inertia emulation controller for MTDC VSCs

In order to achieve an inertial contribution to the onshore AC system from the MTDC VSC converter, a generic inertia emulation controller has been introduced to emulate inertia energy delivery to the AC side of the converter by regulating the DC voltage and hence controlling the effective energy delivery from the DC capacitor(s) on the DC side of the converter. An inertia emulation controller of a similar concept was developed in [11], but this was designed for point-point VSC-HVDC applications. There is a concern that the DC capacitance used for conventional point-point HVDC systems may be too small to generate large enough inertia time constants for MTDC applications and hence additional DC capacitors may be required. With respect to a VSC-MTDC, a larger number of DC capacitors for each VSC terminal within the MTDC system compared to point-point HVDC can be exploited as temporary energy storage for inertia emulation; therefore there is an inherent advantage of applying the controller as developed in [11] for VSC-MTDC systems. This section will introduce the controller design and analyse the value C for the MTDC DC capacitance with regards to the desired emulated inertia time constant H_{VSC} and the degree of DC voltage variation that is reuiqred to deliver this value of inertia.

3.1 Derivation process of the INEC expression

For a sudden mismatch between the mechanical and electrical power in a synchronous machine, its inertia time constant has a significant effect on the rate of change of its rotor angular speed. Taking all the machines in a power system as a whole, the total aggregate machine inertia has a critical impact on the rate of change of grid frequency (ROCOF) during large frequency disturbances. This can be expressed as:

$$\frac{2}{f_0} H \frac{df}{dt} = P_M - P_E = \Delta P_1 \quad \text{(pu)} \tag{8}$$

where f_0 is the nominal frequency in Hz, H is the inertia time constant in sec, P_M is the mechanical power in pu, P_E is the electrical power in pu and ΔP_1 is the kinetic power absorbed by or released from the inertia of the machine during a speed change (in pu).

A dynamic power equation similar to (8) can be found for a VSC with a DC capacitor. When there is a DC voltage variation on the capacitor, the VSC active power output is changed and how much the active power change depends on VSC's DC capacitance. The AC/DC power dynamics can be obtained using the following equation:

$$\frac{NV_{dc}}{\mathrm{S_{VSC}}} C \frac{dV_{dc}}{dt} = P_{in} - P_{out} = \Delta P_2 \quad \text{(pu)} \tag{9}$$

where N represents the total number of capacitors in HVDC or MTDC systems, $\mathrm{S_{VSC}}$ represents the VA rating of the VSC, C represents the MTDC converter terminal capacitance which is the sum of the converter capacitor's capacitance $\mathrm{C_{VSC}}$ and the line capacitance averaged to each VSC terminal $\mathrm{C_{L\_dc}/N}$, P_{in} is VSC power input to the two capacitors in pu, P_{out} is the VSC power output in pu, and ΔP_2 is the dynamic electrostatic power stored or released across both capacitors in pu.

A change of AC grid frequency is indicative of a system power imbalance as expressed in (8). For a VSC with DC capacitors, a change of DC voltage level reflects a change in the active power being supplied by the VSC converter as observed in (9). To equate (8) with (9), a direct link between VSC DC voltage and AC grid frequency can be derived through (10) to (13) together with the emulated inertia time constant H_{VSC}:

$$\frac{2}{f_0} H_{VSC} \frac{df}{dt} = \frac{NV_{dc}}{S_{VSC}} C \frac{dV_{dc}}{dt} \tag{10}$$

Integrating both sides of (10) yields (11) below. This process cancels df/dt and dV_{dc}/dt on the two sides into (11):

$$\int \frac{2H_{VSC}}{f_0} df = \int \frac{NCV_{dc}}{S_{VSC}} dV_{dc} \tag{11}$$

$$\frac{2H_{VSC} f}{f_0} = \frac{NCV_{dc}^2}{2\mathrm{S_{VSC}}} + \mathrm{K_0} \tag{12}$$

$$K_0 = 2H_{VSC} - \frac{NCV_{dc0}^2}{2S_{VSC}} \tag{13}$$

The constant K_0 is the constant of integration which is calculated according to the specified values of H_{VSC}, total combined DC capacitance NC, the nominal DC voltage V_{dc0} and the converter power rating S_{VSC}.

In order to emulate a specific inertia time constant H_{VSC}, equation (12) implies that the DC voltage level in the VSC-HVDC link must vary according to the AC network frequency, although the variation will be non-linear. A large value of H_{VSC} will require a correspondingly large variation in DC voltage and this must be considered in the design of the VSC-HVDC system. The relationship between the emulated VSC inertia time constants and DC voltage variations is derived in [11] as follows:

$$H_{VSC} = \frac{\frac{NCV_{DC0}^2}{2S_{VSC}}\left[\left(\frac{\Delta V_{DC}}{V_{DC0}}+1\right)^2-1\right]}{\frac{2\Delta f}{f_0}} \tag{14}$$

3.2 INEC implementation into MTDC systems

In order to enable an MTDC converter to provide an inertial response to AC grid transients, the overall DC voltage is not expected to be fixed because of the INEC control action on the MTDC network voltage. Because of the possible interaction on the DC network between converters, the MTDC should have only one grid side VSC (GVSC) implemented with the INEC in its DC voltage regulator. The DC voltage reference V_{DC}^* generated for the DC voltage regulating terminal is derived from (12) and (13):

$$V_{DC}^* = \sqrt{\frac{4S_{VSC}H_{VSC}}{NCf_0}\cdot f - K_1} \tag{15}$$

where the constant $K_1 = \frac{4S_{VSC}H_{VSC}}{NC} - V_{DC0}^2$.

To provide inertia response, the DC voltage reference V_{DC}^* for the GVSC with a DC voltage regulator varies with AC network frequency f. The prevailing AC network frequency, which is estimated by the PLL, is used to compute the DC voltage reference through the gains and square root operations based on (9) as shown in Fig. 3. The DC voltage reference should be limited within upper and lower constraints, for example $\pm$ 15% of nominal DC voltage, although the exact figures would depend on insulation requirements, current ratings and PWM functionality.

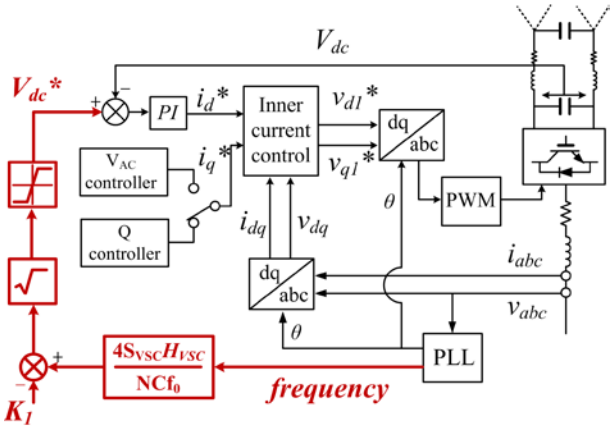

Fig. 3 *The proposed generic INEC for MTDC's VSC*

The implementation of INEC in (9) avoids the processing of frequency differential terms *df/dt* since they have consequent risks of measurement inaccuracies and noise that can threaten stability of the INEC algorithms, especially in response to step transients [17].

3.3 Trade-off between C_{DC} and V_{DC}

Based on (14), Fig. 4 illustrates a range of inertia constants from 0s to 4s along with the associated resultant DC voltage changes for specific frequency changes. The required DC voltage variations on a capacitance of 5 mF and 2 mF at each MTDC VSC terminal are shown in Fig. 4(a) and Fig. 4(b) respectively. It is shown that for a specific frequency deviation, relatively large capacitors can be used in order to limit DC voltage variations and provide the

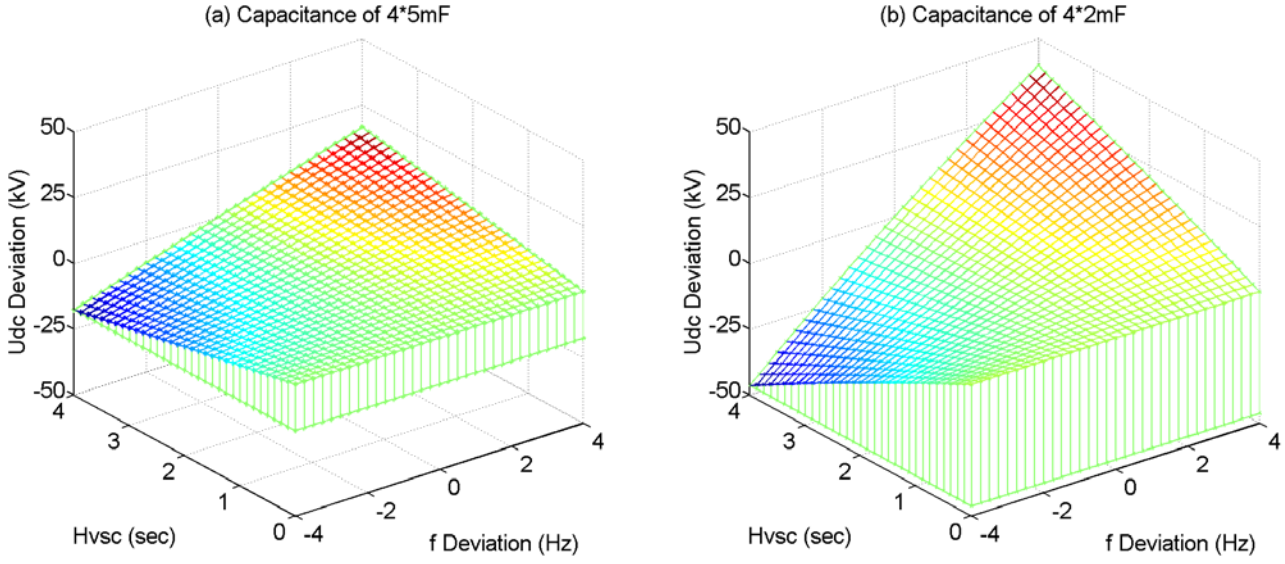

Fig. 4 *Three-dimensional relationship between emulated inertia, frequency and DC voltage deviations from rated value (comparing effect of 2mF and 5mF)*

desired emulated inertia time constants. The tradeoff between capacitor size and maximum allowable DC voltage variation must be taken into account in the design and specification of the system.

4 Simulation results

Simulation scenarios as illustrated in Fig. 1 are carried out in Simulink/Matlab to validate the INEC for the MTDC systems and verify the effectiveness of contributing emulated inertia responses. The four VSCs for the MTDC system are rated at 400 MVA. All converter stations $WVSC_{1,2}$ and $GVSC_{1,2}$ are described using detailed switch models of a two-level voltage source converter, with their AC side filters tuned to attenuate switching frequency harmonics and their sidebands. The lines that form the DC network are modelled using nominal π configuration with parameters presented in Table A, and this is sufficient considering the scope of this paper. However, for DC fault studies, the use multiple π sections is necessary to avoid over-estimation of the DC fault current (but this is outside of the scope of this paper).

On the offshore side, the two DFIG based WF_1 and WF_2 are simulated respectively as one lumped DFIG model with its turbine aerodynamic model, drive train system, induction generator model and back-to-back PWM conversion system. On the onshore side, the 600 MVA rated SG_1 and 200 MVA rated SG_2 are represented by the seventh-order model with IEEE parameters [15]. Their inertia time constants are 3.3s and 3.2s, respectively. The 400 kV Transmission networks interconnect two MTDC GVSCs and two SG with passive load banks $Load_{1,2,3}$, with specific lengths as shown in Fig. 1 and impedance parameters as presented in Appendix Table B.

4.1 Load increase

Figs. 5 shows the simulation comparisons between $GVSC_1$ with a DC voltage controller which regulates its node DC voltage level constant at 301 kV (H_{VSC1}=0), and the same $GVSC_1$ with the INEC which emulates an inertia time constant of H_{VSC1}=3s and H_{VSC1}=1.5s. The load increase is initiated by switching on $Load_3$ of 50 MW, representing 5% of the total load. Fig. 5(a) illustrates the voltage change resulted by the sudden load increase, with minor voltage drop of 0.02 pu observed. As shown in Fig. 5(b)(c), MTDC terminal DC voltage levels by the traditional control remains constant for the sudden load change, whereas those equipped with INEC are controlled to drop. As observed in Fig. 5(d), a rapid power increase from $GVSC_1$ indicating its inertia contribution from the INEC action, whereas $GVSC_1$ with the traditional DC voltage controller remains the same. Due to the inertial interactions among

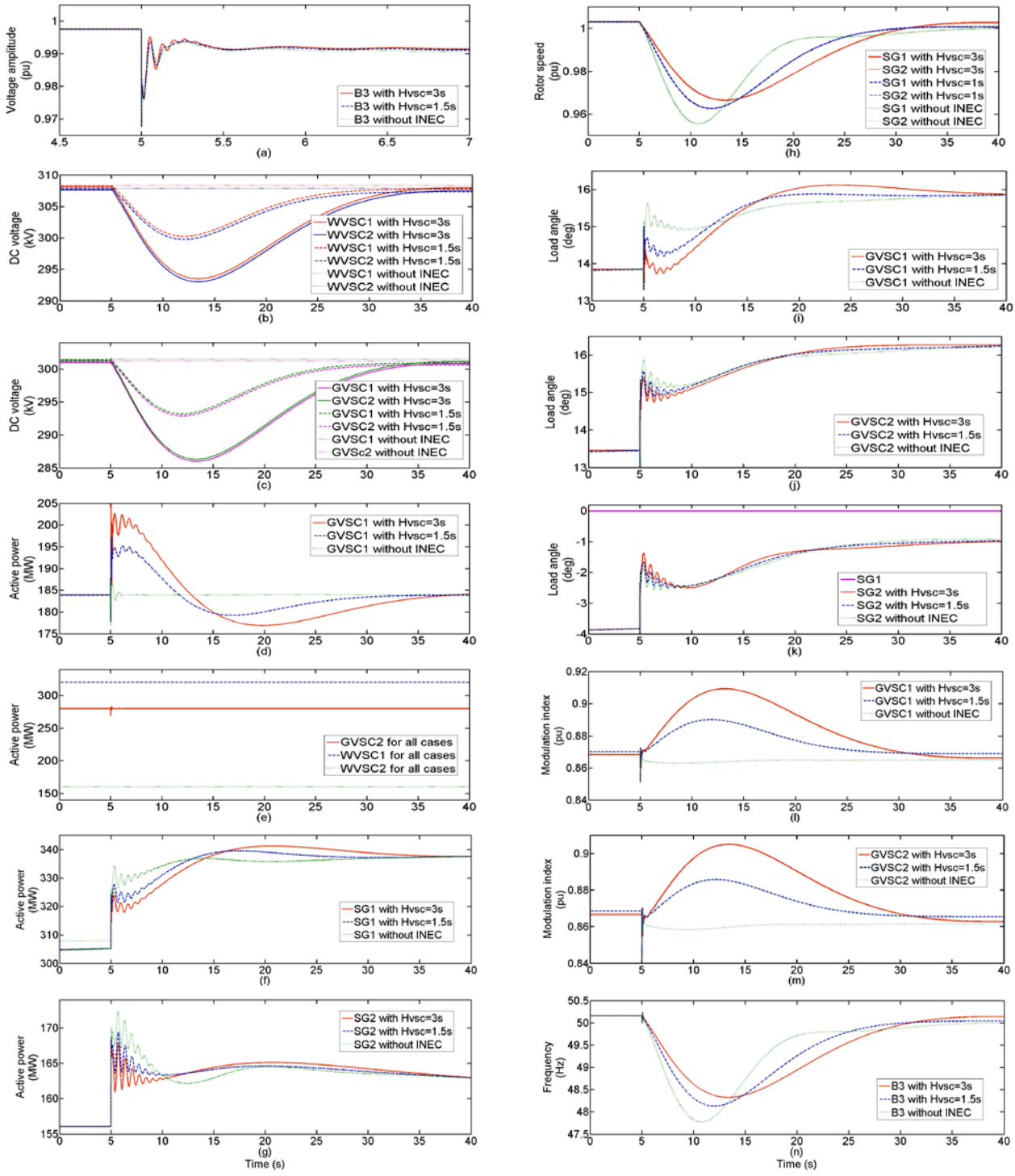

Fig. 5 *5% Load increase by switching on Load$_3$*

the MTDC's GVSC$_1$ and two SGs, the output active power from SG$_1$ and SG$_2$ are significantly reduced as observed in Fig. 5(c)(d). By comparison between the active power outputs of GVSC$_1$ and each of the two SGs, similarities are found in the first 2s after the load change. However, SG$_1$ and SG$_2$ possess primary controllers (steam turbine governors in this case) leading to a subsequent increase of their power outputs to meet the system demand. In

contrast, $GVSC_1$ provides a short-term "pure" inertial active power impulse using the energy stored in the MTDC capacitors. The benefits of the inertia contribution from $GVSC_1$ are evident from the rotor speed of each of the SGs as shown in Fig. 5(h), the voltage and load angles (with respect to SG_1's electromotive force angle) of the GVSCs and SGs as shown in Figs. 5(i)(j)(k) respectively, as well as the network frequency drop at busbar B_3 as shown in Fig. 5(n). Despite the short period of inertia contribution by the MTDC, it significantly improves the frequency performance of the supplied AC multi-machine system.

Fig.5(l)(m) present the modulation indices for converter stations $GVSC_1$ and $GVSC_2$, and it can be observed that the modulation indices of both converters are equally varied between 0.84 to 0.91 as the load is changed. Fig. 5(e) shows that the active powers of $WVSC_1$, $WVSC_2$ and $GVSC_2$ do not respond to the load increase. This verifies that the INEC decouples disturbances from the onshore AC grid side to the offshore wind farm side, while still contributing an emulated inertia; this is an attractive feature of the INEC. The INEC can of course also be applied to $GVSC_2$; this will be studied in Section 4.2 which relates to testing performance under fault conditions.

4.2 Fault study

Figs. 6 show the simulation results from fault studies with the INEC applied to $GVSC_2$ (and with three separate inertias of H_{VSC2}=3s, 1.5s and 0). The fault is simulated at Busbar B_3 as illustrated in Fig. 1, and has a duration of 140 ms before being cleared – in practice, fault clearance may be faster than this, but this duration has been chosen to simulate worst case fault clearance conditions according to [10]. As described in [11], the restrained capability of the INEC by solid faults due to the VSC current saturation, in this case only the resistive fault which results in a 0.5 pu voltage amplitude drop at B_3 as shown in Fig. 6(a), is studied.

It is clearly shown in Fig. 6(b)(c) that DC voltage levels for each of the four VSC nodes are not affected by the fault when conventional non-inertial control schemes are applied, whereas the DC voltage level changes for those results where $GVSC_2$ is equipped with INEC and H_{VSC2}=3s and H_{VSC}=1.5s as shown in Fig. 6. Through the active power interactions between $GVSC_2$ and two SGs as shown in Figs. 6(d)(f)(g) respectively, the rotor speed variations and frequency variations at busbar B_3, as illustrated in Fig. 6(h) and (n) respectively, are significantly damped and postponed by larger emulated inertia provided by $GVSC_2$. The small load angle variations for the case with H_{VSC2}=3s than those with H_{VSC2}=1.5s and 0, observed in Figs. 6(i)(j)(k) indicating the stabilising effect of the

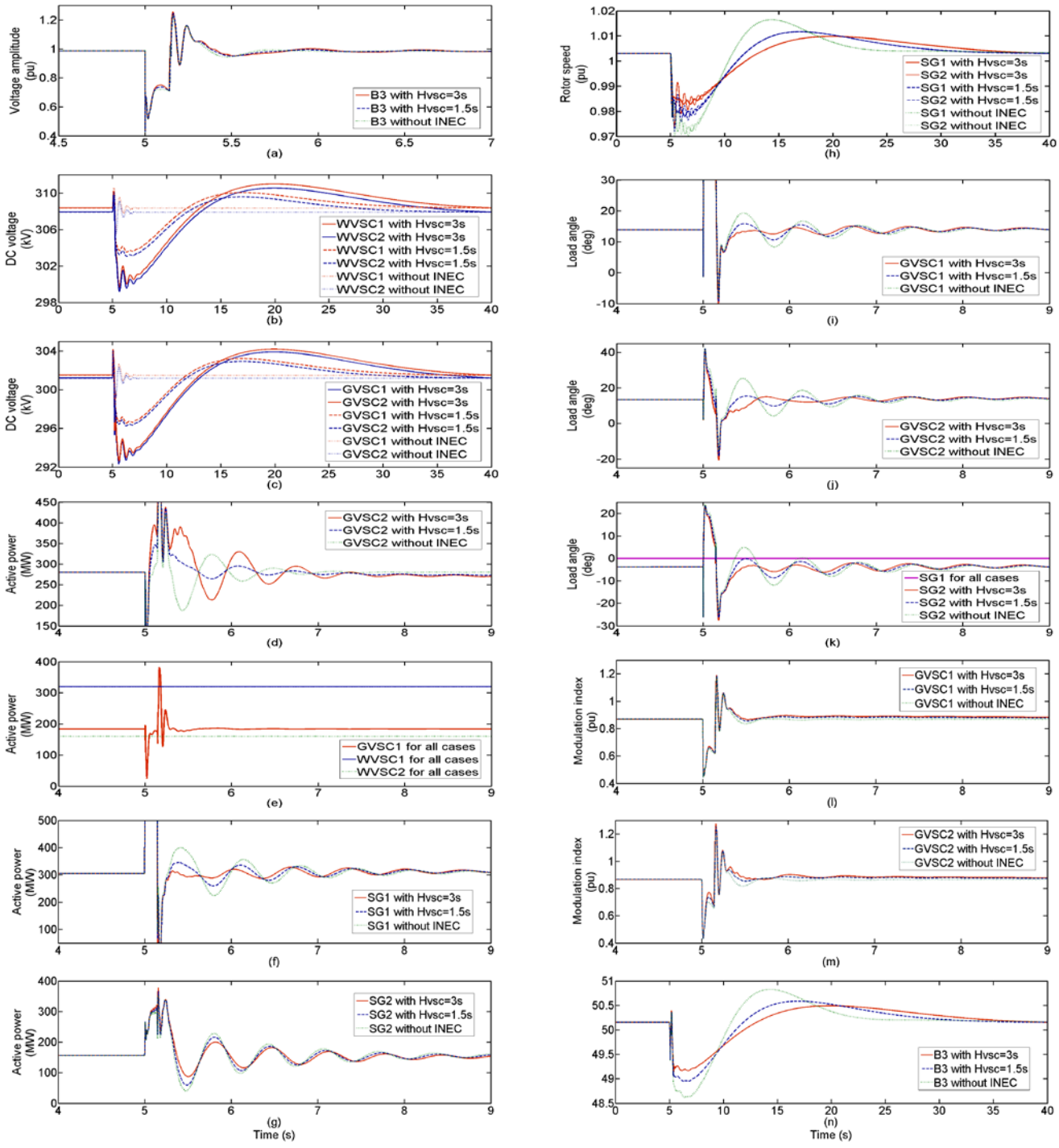

Fig. 6 *Resistive fault test (30% voltage drop for 140ms)*

INEC for the fault test. As observed in Fig. 6(a) the grid voltage at busbar B3 increases to 1.2pu for a short time after fault clearance due to load rejection and reactive power mismatch. This results in the modulation index references of GVSC1 and GVSC2 being temporarily beyond the maximum value of 1pu for PWM as observed in Figs. 6(l)(m). In the control system, modulation indices are always limited to 1pu to avoid unacceptable over-modulation, whereas here the modulation index references are presented without applying the limit in order to

clearly show the degree of INEC intended modulations. Throughout the whole simulation process presented in Fig. 6, it appears that the GVSCs with the INEC help to minimise the system disturbances arising from the fault. The active power of $WVSC_1$, $WVSC_2$ and $GVSC_1$ remain the same for three cases, as shown in Fig. 6(e).

5 Conclusion

This paper has described a generic inertia emulation controller (INEC) for multi-terminal HVDC (MTDC) system application, as a follow-up activity from its implementation on a point-to-point HVDC system, as presented in [11]. The INEC allows a MTDC grid side converter to contribute an inertial response, by varying DC voltage levels to access and exchange the electro-static energy stored in DC link capacitors with an AC grid. The system does not require any modification to the MTDC hardware. The presented simulation results have shown that the INEC possesses the following features:

i) It facilitates damping of synchronous generators' rotor speed variations during system disturbances (e.g. demand changes, temporary faults) by supplying and absorbing compensating energy to and from the AC system as required;

ii) Power system frequency deviations as well as busbar load angle deviations during system disturbances are effectively stabilized by the INEC;

iii) The INEC retains the decoupling feature of VSCs, which isolates AC grid disturbances from offshore weak AC power systems used for wind farm energy collection.

The study scenario assumes a network with comparable grid and off-shore generation capacity to allow the effectiveness of the inertia contribution control concept on VSC-MTDC system to be assessed. Future work will be required to explore how the INEC can be implemented on existing systems in more detail, and how the operation of the INEC can be perfected under conditions where there are high grid voltage harmonics and under unbalanced conditions.

6 References

[1] Lalor, G., Mullane, A., O' Malley, M.: 'Frequency control and wind turbine technologies', *IEEE Trans. Power. Syst.*, 2005, **20**, (4), pp. 1905–1913

[2] Conroy, J., Watson, R.: 'Frequency response capability of full converter wind turbine generators in comparison to conventional generation', *IEEE Trans. Power Syst.*, 2008, **23**, (2), pp. 649–656

[3] Mokadem, M. E., Courtecuisse, V., Saudemont, C., Robyns, B., Deuse, J.: 'Experimental study of variable speed wind generator contribution to primary frequency control', *Renew. Energy*, 2009, **34**, pp. 833–844

[4] Kayikci, M.; Milanovic, J.V.: 'Dynamic Contribution of DFIG-Based Wind Plants to System Frequency Disturbances', *IEEE Trans. on Power Syst.*, 2009, **24**, (2), pp. 859-867

[5] Miao, Z., Fan, L., Osborn, D., Yuvarajan, S.: 'Wind farms with HVdc delivery in inertial response and primary frequency control', *IEEE Trans. Energy Convers*., 2010, **25**, (4), pp. 1171-1178

[6] Phulpin, Y.: 'Communication-Free Inertia and Frequency Control for Wind Generators Connected by an HVDC-Link', *IEEE Trans. Power Syst.*, 2012, **27**, (2), pp. 1136-1137

[7] Zhu, J., Booth, C.D.: 'Future multi-terminal HVDC transmission systems using Voltage source converters'. Proc. Int. Univ. Power Eng. Conf., Cardiff, U.K., 2010, pp. 1-6

[8] Lu, W.X., Ooi, B.T.: 'Multiterminal LVDC system for optimal acquisition of power in wind-farm using induction generators', *IEEE Trans. on Power Electron.*, 2002, **17**, (4), pp. 558-563

[9] Jovcic, D., Strachan, N.: 'Offshore wind farm with centralised power conversion and DC interconnection', *IET Gen., Trans. & Dist.*, 2009, **3**, (6), pp. 586-595

[10] National Grid UK: 'The GB Grid code', http://www2.nationalgrid.com/UK/Industry-information/Electricity-codes/Grid-code/The-Grid-code/

[11] Zhu, J., Booth, C.D., Adam, G.P., Roscoe, A.J., Bright, C.G.: 'Inertia Emulation Control Strategy for VSC-HVDC Transmission Systems', *IEEE Trans. on Power Syst.*, 2013, **28**, (2), pp. 1277-1287

[12] Xu, L., Yao, L.Z.; Sasse, C.: 'Grid Integration of Large DFIG-Based Wind Farms Using VSC Transmission', *IEEE Trans. on Power Syst.*, 2007, **22**, (3), pp. 976-984

[13] Green, T.C., Prodanovic, M.: 'Control of inverter-based micro-grids', *Electric Power Systems Research*, 2007, **77**, pp. 1204-1213

[14] Feltes, C., Wrede, H., Koch, F., Erlich, I.: 'Fault ride-through of DFIG-based wind farms connected to the grid through VSC-based HVDC link'. PSCC 16th Power System Computation Conf., 2008, pp. 1-7

[15] Anderson, P., Fouad, A.A.: 'Power System Control and Stability', The Iowa State Univerity Press, 1977

[16] Novotny, D. W., Lipo, T. A.: 'Vector Control and Dynamics of AC Drives', Clarendon Press, 1996

[17] Bennett, S., 'Development of the PID controller', *IEEE Trans. Control Syst.*, 1993, **13**, (6), pp. 58–62

[18] Adam, G. P., Williams, B. W., "Half and Full-Bridge Modular Multilevel Converter Models for Simulations of Full-Scale HVDC Links and Multi-terminal DC grids," Accepted for publication in a future issue of IEEE Journal of Emerging and Selected Topics in Power Electron., 2014

[19] Adam, G. P.: 'Voltage Source Converter: Modulation, Control and Applications in Power Systems', CreativeSpace, 2013

7 Appendix

Table A Parameters for the DC system

Item	*Value*
Rated MTDC VSC power S_{VSC}	400 MVA
Nominal DC voltage V_{DC0}	±150 kV (300 kV)
Converter side RMS AC voltage	150 kV
DC line impedance per km	9e-3Ω, 3.3e-4H, 3.1e-7F
VSC DC capacitor C_{dc}	5mF
Total number of capacitors N	4
Switching frequency f_{sw}	1350 Hz
Power Rating of Wind Farm WF_1	380 MVA
Power Rating of Wind Farm WF_2	360 MVA

Table B Parameters for the AC grid system

Item	*Value*
AC network line-to-line voltage	400 kV
AC network impedance per km	5.29e-2Ω, 1.4e-3H, 8.7e-9F
SG_1 rated power	400 MVA
SG_1 Terminal line-to-line voltage	13.8 kV
SG_1 inertia time constant	3.3 s
SG_1 turbine time constant T_w	2.67 s
SG_1 servomotor time constant T_a	0.1 s
SG_1 exciter time constant	0.001 s
SG_2 rated power	200 MVA
SG_2 Terminal line-to-line voltage	13.8 kV
SG_2 inertia time constant	3.2 s
SG_2 turbine time constant T_w	2.43 s
SG_2 servomotor time constant T_a	0.07 s
SG_2 exciter time constant	0.001 s

Table C Parameters for the offshore AC system

Item	*Value*
WTG Rating	4 MVA
Rated wind speed	12 m/s
Rotor diameter	110 m
Wind turbine inertia $H_{turbine}$	3.5 s
Wind power generator $H_{generator}$	0.65 s
Stator/rotor/mutual L_s, L_r, L_m	0.09385, 0.09732, 3.96824
Stator/rotor R_s, R_r	0.00536, 0.00519
VSC rating	1 MVA
WTG VSC capacitance C_{dc}	1.6 F